Journal of Visualization, Vol. 1, No. 2 (1998) 171-181

Development of Particle Image Velocimetry for Multiphase Flow Diagnostics

Palero, V.* and Arroyo, P.*

* Universidad de Zaragoza, Departamento de Física Aplicada, Facultad de Ciencias, 50009 - Zaragoza, Spain.

Received 12 March 1998.
Revised 20 July 1998.

***Abstract*:** This paper discusses the suitability of PIV for measuring simultaneously the velocity field of every phase and the size and concentration field of the disperse phases in multiphase flows. Velocity and disperse phase information are both inferred either directly from the Young's fringe pattern (far field diffraction function) or from its 2-D Fourier transform (autocorrelation function). In the first case, the velocity is inferred from the orientation and spacing of the fringes while the disperse phase size is inferred from the size of the diffraction halo that modulates the fringes. In the second case, the velocity and particle shape are related to the position and shape of the strongest autocorrelation peaks, respectively. Particle sizes are used to discriminate between phases on the velocity measurements. The technique has been demonstrated on a high speed air-particle flow, where the potential for determining air velocities and particle size and velocities are shown.

***Keywords*:** particle image velocimetry, multiphase flows, particle sizing, laser velocimetry.

1. Introduction

The majority of flows of industrial relevance are essentially unsteady and three-dimensional multi-phase flows. A good knowledge of the flow structure, including the behavior and interaction of all the phases, is vital in many areas of practical importance such as the safe and efficient design of combustion systems, pollution control and many others. In recent years, particle image velocimetry (PIV) has acquired great relevance in experimental fluid mechanics as a means of obtaining an instantaneous map of the two in-plane components of a velocity field (Adrian, 1991). PIV is based on a multiple exposure recording of a two-dimensional section of a seeded flow field. The flow section is usually illuminated by a pulsed sheet of laser. The light scattered by the seed particles (or any other scatterers in the flow) produces multiple particle images on the recording, whose separation is directly related to the velocity at any particular point. Up to date, PIV has been applied mainly to single-phase flows, where the fluid is artificially seeded with small size tracers. The application to multiphase flows is more complex because its study requires the knowledge of the velocity map for every phase independently. Furthermore, information about the concentration and size of the disperse phases is very useful in multiphase flow diagnostics. This information is intrinsically contained in standard PIV recordings and could be inferred from them using the appropriate analysis.

Recently, a few applications of PIV to two- and three-phase flows have been reported (Hassan and Canaan, 1991; Hassan et al., 1992; Liu and Adrian, 1992; Chen and Fan, 1992; Palero et al., 1995; Jakobsen et al., 1996). All these applications address the issue of simultaneously, but independently, measuring the velocity field of all the phases being particle tracking velocimetry the preferred technique to analyze the disperse phases. Particle image sizes are used for the phase separation but only Palero et al. (1995) try to quantitatively measure the disperse phase sizes. Albert and Farrell (1994) and Coil and Farrell (1994) propose a method for particle sizing in a spray using a PIV recording.

This paper will study a method, presented earlier by the authors (Palero et al., 1995), of using PIV for measuring simultaneously the velocity field of every phase and the size and concentration field of the disperse phases in multiphase flows.

2. PIV for Multiphase Flow Diagnostics

The multiphase flow diagnostics uses a PIV photographic recording of a fluid plane. The photograph consists of multiple equally spaced images of each particle, whose spacing is proportional to the particle velocity. In the following, we will work with spherical particles whose images appear as disks, having a diameter proportional to the particle diameter.

The PIV photograph is analyzed, one point at a time, using a Young's fringe method (Arroyo et al., 1988). The experimental setup for this analysis is shown in Fig. 1. Basically, an unexpanded He-Ne laser beam illuminates a small region (about 1 mm in diameter) of the photograph. The photograph is placed on a translation stage, whose movement is controlled with a computer, to obtain a sequential illumination of portions of the film. The lens collects the light diffracted by the particle images on the illuminated region. This diffracted light produces, in the focal plane of the lens, a pattern known as Young's fringes (Fig. 1(b)). A CCD camera is used to record the Young's fringes and a black stop is placed in the origin to block the undiffracted light.

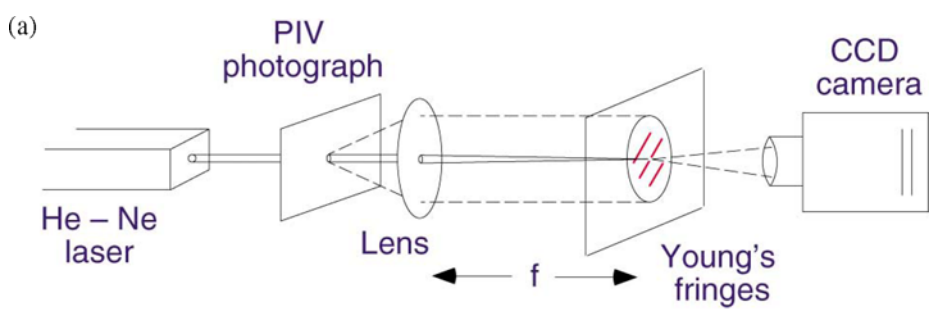

Fig. 1. (a) Experimental setup for the analysis of PIV photographs; (b) typical Young's fringe pattern.

A simple theoretical analysis allows us to describe the intensity of the Young's fringes, $I(x, y)$, as

$$I(x,y) = S(x,y)\, H(x,y) \tag{1}$$

where the interference term, $S(x, y)$, contains all the information about the velocity while the diffraction halo, $H(x, y)$, contains the information about the shape of the particles.

When N exposures are taken on the photograph, $S(x, y)$ can be expressed as

$$S(x,y) = t^2 \frac{\sin^2(\pi N M T \vec{v}.\vec{r}/\lambda f)}{\sin^2(\pi M T \vec{v}.\vec{r}/\lambda f)} \tag{2}$$

where t is the time for each exposure, T is the time interval between the exposures, $\vec{v}$ is the velocity vector, $\vec{r}$ = (x,y) is the position vector, M is the magnification of the imaging system, λ is the wavelength of the interrogation beam and f is the focal length of the lens. Equation (2) represents a series of fringes, which are perpendicular to the velocity vector and whose spacing is inversely proportional to the magnitude of the velocity. The fringes become brighter and sharper when N increases.

When particle images are circular and uniform in size, H(x,y) is an Airy disk pattern given by

$$H(x,y) = cN' \left[\frac{\pi D^2}{4}\right]^2 \left[\frac{2\,J_1(a)}{a}\right]^2 \tag{3}$$

with

$$a = \frac{\pi r D}{\lambda f} \tag{4}$$

where c is a constant, $J_1(a)$ is a first order Bessel function, $r = \sqrt{x^2 + y^2}$, D is the particle image diameter and N' is the number of particles. The function represented by Eq. (3) has a maximum at the origin and decreases until it reaches a zero value at $r = 1.22\,\lambda f / D$, that limits the area where fringes can be seen.

In the example shown in Fig. 1(b), the shape of the diffraction halo is elongated. This means the particle image is not circular, being longer in the direction of the velocity vector and shorter in perpendicular. However, in this case, this elongated image was produced by a too long exposure time rather than by an elongated particle.

2.1 Fringe Analysis for Velocity Measurements

The velocity in the illuminated area can be obtained from the analysis of the Young's fringes using two different methods: 1-D averaging and 2-D Fourier transform

In the 1-D averaging method (Arroyo et al., 1988), the fringe orientation and spacing are calculated. First of all, the fringe orientation is obtained by looking for the radial line with the maximum total intensity. Then, the fringe intensity is averaged along lines parallel to the fringes. This produces a 1-D signal whose frequency, which is obtained by a 1-D Fourier transform, is proportional to the magnitude of the velocity.

The 2-D Fourier transform of the Young's fringes produces the autocorrelation function of the illuminated portion of the film (Adrian, 1991). In this case, the velocity vector is related to the position vector of the strongest autocorrelation peak that is not in the origin.

2.2 Fringe Analysis for Particle Size Measurements

The particle size can be obtained from the analysis of the Young's fringes using the same two methods as for velocity calculation.

In the 1-D averaging method, the radial line with the maximum local intensity is used. This line corresponds to constant values of $S(x, y)$, being the intensity changes along the line given by the $H(x, y)$ term. The particle size is inferred by fitting this line to the function shown in Eq. (3) (Fig. 2(a)). Let us note that only the particle size in a direction perpendicular to the velocity vector can be measured. In any other direction the function $H(x, y)$ cannot be isolated from $I(x, y)$.

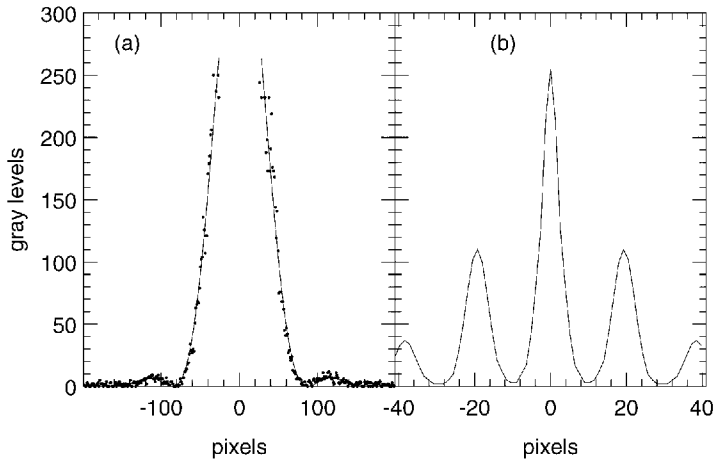

Fig. 2. Typical signals from the particle size diagnostic: (a) intensity line from the diffraction halo; (b) intensity line from the autocorrelation plane.

In the autocorrelation plane, the shape of the autocorrelation peak is directly related to the particle image characteristics. When the particle images are constant intensity disks, the autocorrelation peaks are cones. The base of these cones is a disk with diameter $2D$ while the diameter of the mid-height disk is D. If the particle images are elongated, the section of the autocorrelation peaks will also be elongated. If the intensity on the particle images is a Gaussian function, the section of the autocorrelation peaks will also be Gaussian. Thus, not only particle diameter but particle shape can be obtained by this method. Figure 2(b) shows the autocorrelation function in the direction of the velocity. Particle diameters are inferred by measuring the width of the peaks along this line. In practice, it is the width at mid-height the parameter being used because it is less affected by noise than the width at the base.

Let us note that we are using the dependence of intensity with position for particle sizing, while for velocity measurements only maxima intensity positions are important. This means that it is essential for particle sizing to use a CCD camera whose electronics does not change the linearity of the CCD sensor.

Some parameters that may affect differently both techniques are the intensity of the laser beam, the undiffracted light and non-uniform local velocities. If the intensity of the laser beam is kept low so as the Young's fringes do not saturate the camera, both techniques will not be affected by how low the intensity is. If the intensity is higher, the autocorrelation peak will show smaller sizes than expected because the Airy disk of the diffraction halo will be truncated. However, since we removed the saturated pixels on the fitting to the Bessel function, the effect of the high intensity is mainly to diminish the number of points in the fitting. This may produce more errors in the measurement, depending on the noise of the data, but not any systematic deviation from nominal values. The undiffracted light that lies on the origin of the fringes has a similar effect on this method but it does not affect to the autocorrelation peak. Finally, non-uniform local velocities increase the width of the autocorrelation peaks while not affecting the width of the central peak. They also do not affect the Bessel fitting.

2.3 Multiple Phase Separation

The different phases of the flow are distinguished by sizing their respective particle images. Velocity and particle size are extracted at each interrogation point of the PIV photograph by analysing the corresponding Young's fringe pattern, as explained in Ssections 2.1 and 2.2. The measurement will be associated to the disperse phase if the calculated size is above a certain value or to the continuous phase, otherwise.

The relationship between diffraction intensity and particle size is used to increase the amount of velocity vectors obtained for the continuous phase, as it is explained in the following. As it has already been pointed out (Jakobsen et al., 1996), when the interrogation area contains one or more tracks of big particles, the measured velocity corresponds to the big particles (instead of the continuous phase) because the diffraction intensity from the big particles is much higher than that from the small scatterers as shown in Eq. (3). The removal of the disperse phase signal is done here by increasing the intensity of the laser used in the analysis. The diffracted light from the big particles will extend to a smaller area than the light from the small particles and will likely saturate the CCD camera. If a black spot, bigger than the one used to remove the undiffracted light, is placed at the center of the Young's fringes, the signal from the big particles will be removed and only the continuous phase signal will be measured. On the other hand, for measuring the velocity field of the disperse phases, a low laser intensity will be used on the analysis. In this way the diffracted light by the small particles will be kept below the noise threshold and only the big particles will contribute to the Young's fringe pattern.

With this procedure, the PIV photograph has to be analyzed twice, one for measuring the continuous phase and another for measuring the disperse phase. Since the disperse phase particles are, in general, sparsely located not all the interrogation areas will contain this phase and the exact location of each particle will be of interest. Thus, when measuring the disperse phase, only fringe pattern with gray levels above a certain threshold are analyzed. This allows to interrogate areas more closely spaced for a more accurate location of the disperse phase particles. With this process, the same particle image can appear on several close areas, being the mean position of those areas taken as the particle image position.

The intensity of the diffracted light together with the size information is used to infer the number of disperse phase particles within the interrogation area.

The whole procedure will work for particle image sizes up to one fourth of the interrogation area diameter and for less than two disperse phase particles per area (concentration about one tenth of the optimum continuous phase tracer concentration).

2.4 Particle Imaging

Up to now, we have assumed ideal conditions for particle images. There are several factors that may give less than ideal conditions for this particle imaging. Let us note we will limit here to spherical particles and illumination with a light sheet beam that travels from left to right.

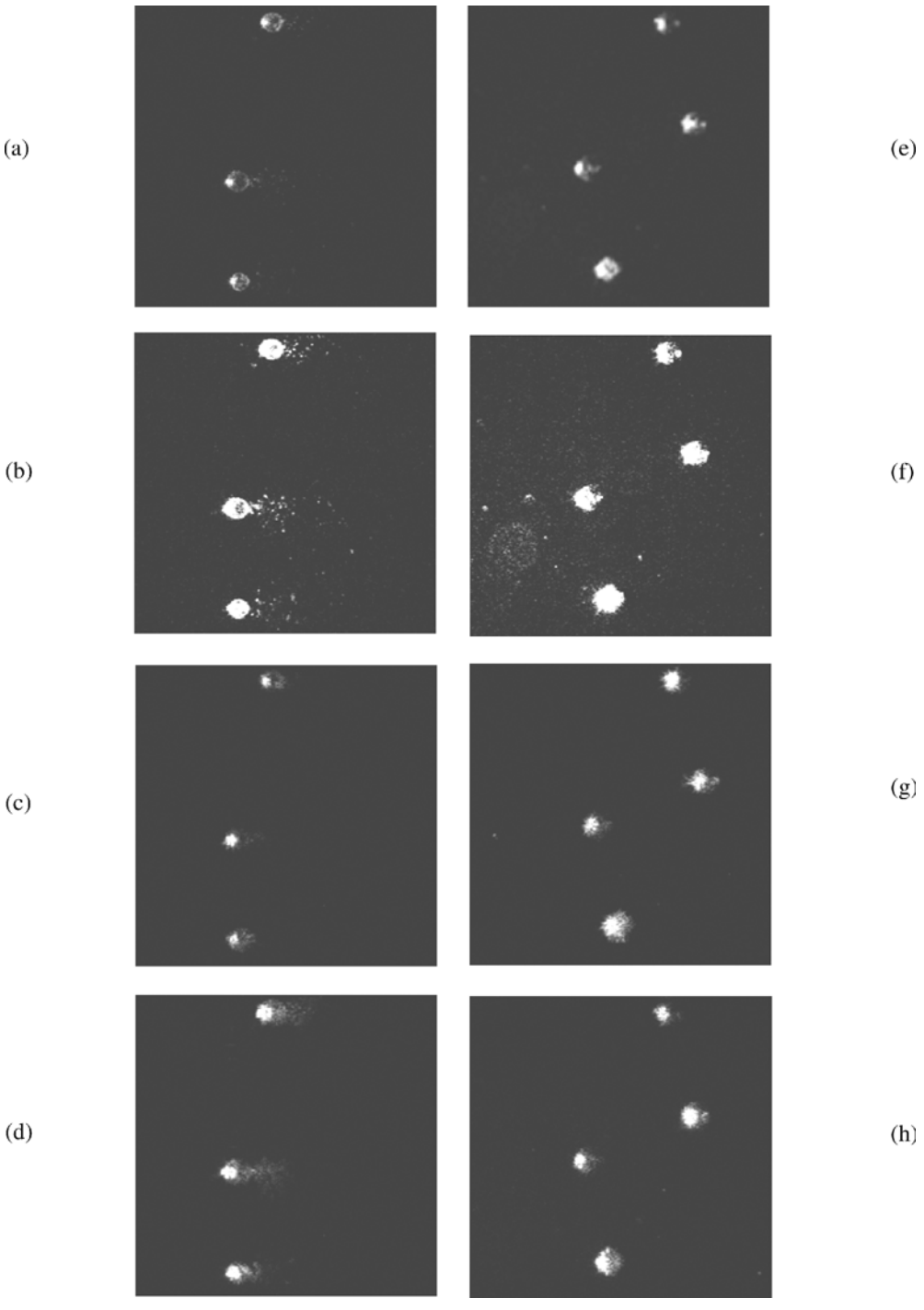

Fig. 3. Typical particle images obtained from uncoated glass spheres in air (a-d) and silver coated glass spheres embedded on a transparent polymer (e-h). Particle diameter is ~100 μm. (a) and (e) Unsaturated and focused particle images; (b) and (f) saturated focused particle images; (c) and (g) particles are 250 μm behind the focused plane; (d) and (h) particles are 250 μm in front of the focused plane.

The particle imaging is obtained by collecting the light dispersed by the particles at 90° from the illumination direction. The intensity and wavefront of this light depends, firstly, on the type of particles. When the particle is a droplet of a fluorescent liquid, the particle image will be a disk since the droplet is the source of the fluorescent light. If the particle is not transparent and its surface acts as a diffuser, the beam will illuminate only the left half of the particle. Thus the particle image will be half a disk. However, due to the light diffused by other particles the right half can be recorded, too, but with lower intensity (Fig. 3(e)). Finally, for a particle that partially reflects and partially transmits the incident light, the reflected light comes out as a divergent beam whose focus is inside the particle. In this case, one bright spot can be seen on the left side of the particle. Again a less bright spot can be seen on the right due to either reflections of the light transmitted through the particle and/or of the light reflected by other particles (Fig. 3(a)). A small amount of light is also seen all around the particle. In conclusion, the images of spherical particles are far from being disks. However, all of them have some light on the boundary of a perfect disk. This means that, if the amount of energy recorded from each particle is increased until the recording media (film or CCD sensor) saturates a little, the particle image will look like a disk (Figs. 3(b), (f)) although its diameter will be bigger than the nominal value.

Particle images are also affected by the particle defocusing. Since the width of the laser sheet is typically 1 mm, not all the particles will be perfectly focused. Figures 3(c), (d), (g), (h) show the images obtained when the particles are placed 250 μm behind (Figs. 3(c), (g)) or 250 μm in front of the focused plane (Figs. 3(d), (h)). The images were taken with a CCD camera using a Micro Nikkor 55 mm lens in an inverted position with $f/4$. The magnification of the system is such that each pixel of the CCD sensor corresponds to 3 μm. It can be seen that the size and intensity of the left bright spot increases more for the particles in front of the focused plane. However, when the images are saturated its size is similar to the best focused images (Figs. 3(b), (f)).

Finally, let us note that Fig. 3 also shows that images of light diffusing particles will reproduce more faithfully the particle geometrical characteristics than images of light reflecting particles.

3. Experimental Testing

The performance of the particle size diagnostics was studied using several test objects.

Firstly, we have looked at the diffraction produced by a pinhole using the analysis system shown in Fig. 1(a). The pinhole is situated in the place of the PIV photograph. The diffraction pattern, which is a perfect Airy disk, is acquired by the CCD camera. The gray levels along eighteen 10°-spaced radial lines are read. Each line is then fitted to a Bessel function. Figure 4 shows the results obtained for two different size pinholes for several

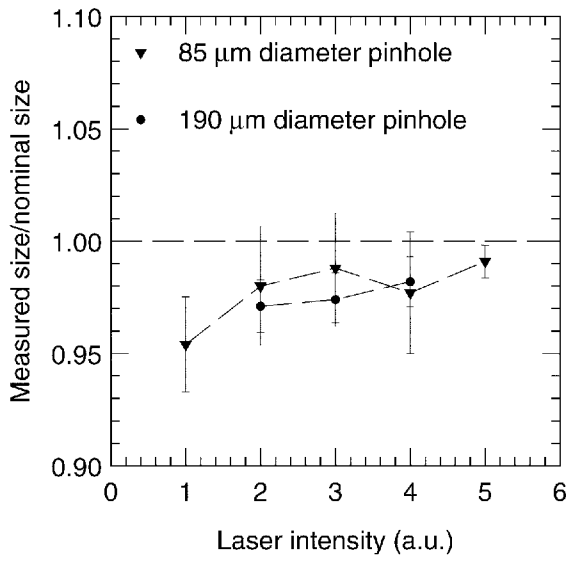

Fig. 4. Dependence of the measured diameter for two pinholes on the laser intensity used in the analysis (a.u. means arbitrary units). Each dot and its error bar represent the average value and the standard deviation of a 18-data set obtained from analysing the diffraction halo along different radial lines.

different intensities of the laser used in the analysis. Each dot and its error bar represent the average value and the standard deviation obtained from the 18 data. It can be concluded that average sizes are obtained with an error of 2%, being 4% the variation due to the laser intensity. This gives an idea of the order of magnitude of the errors we will get in the best case.

The experiment also showed that the output of our digital image processing system was not linear. CCD devices are, in general, linear but the electronics of the video signal and the frame grabbers may introduce nonlinearities in the global response of the system. The CCD we are using is specifically designed for surveillance and is made nonlinear on purpose so as to have a wider range of light levels. The nonlinearities produced signals that could not be fitted well to a Bessel function. This was resolved by linearising the video signal through the look out tables of the frame grabber using the method proposed by Quiroga et al. (1995). Another defect of our processing system is that the pixels of the CCD sensor are rectangular. The frame grabber gives an output with 512×512 nominally square pixels. However, we have checked that there is a 3% difference between the horizontal and the vertical pixel dimensions, that we have taken into account in our analysis software.

Next, we have used several test objects consisting on different size spherical black dots printed by computer on white paper. This object was photographed at a magnification of 0.1 on the same film used for PIV photographs. The recording is then looked through the analysis system shown in Fig. 1(a). The first object contains single dots with sizes between 0.1 and 2 mm (10 to 200 μm on the recording). Figure 5 shows the results obtained with the same analysis procedure used for the pinholes, but limited to a fixed laser intensity. The average values differ in less than 7 μm from nominal sizes with typical standard deviations of 4 μm. The next object contains groups of four dots. The dots in each group have the same diameter, ranging from 0.2 to 1 mm (20 to 100 μm on the recording), at distances of 2 mm (200 μm on the recording). Figure 6 compares the results obtained from the diffraction halo analysis and from the autocorrelation peak analysis. Only one data can be obtained from the halo analysis. Only the size on the horizontal direction has been measured from the autocorrelation analysis. The results obtained by the two techniques agree well. However, lets note that care has been taken so that the fringe pattern is not saturated when using the autocorrelation analysis. Let us also note that measured sizes are significantly bigger than nominal sizes for nominal particle diameters below 40 μm. We attribute this to inaccuracies in the test object itself, due to the difficulties in printing and photographing such small dots.

The effect of particle defocusing and film saturation on the particle imaging step has been studied using a solid object of silver coated glass spheres embedded on a transparent polymer. The nominal size of the particles range from 90 to 106 μm and they all were in the same plane inside the polymer. This plane was photographically recorded, deciding by eye when the particles were focused. A Micro Nikkor 55 mm lens with aperture *f*/4 set up at M=1 was used for the recording. Other recordings were taken after displacing the object by 250 μm at both sides

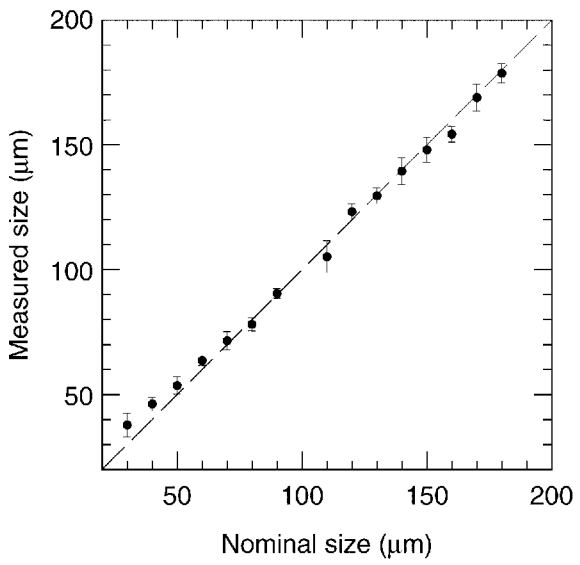

Fig. 5. Measured particle sizes, as a function of nominal values, from a photograph of single black dots printed on a white paper. Each dot and its error bar represent the average value and the standard deviation of a 18-data set obtained from analysing the diffraction halo along different radial lines.

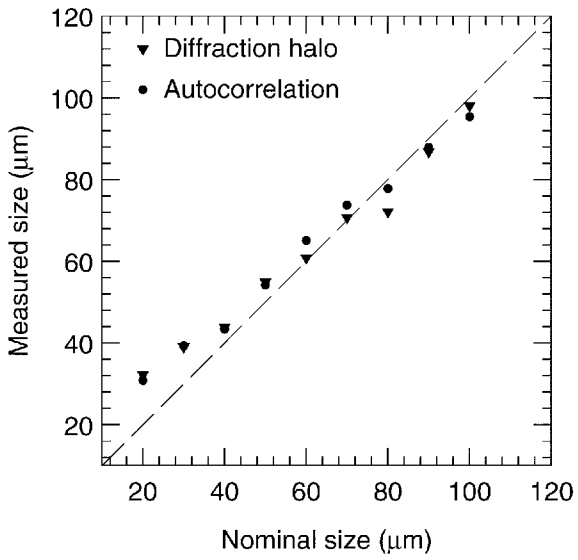

Fig. 6. Comparison of the diffraction halo analysis with the autocorrelation plane analysis. The data were obtained from a photograph of groups of four equally spaced black dots printed on white paper.

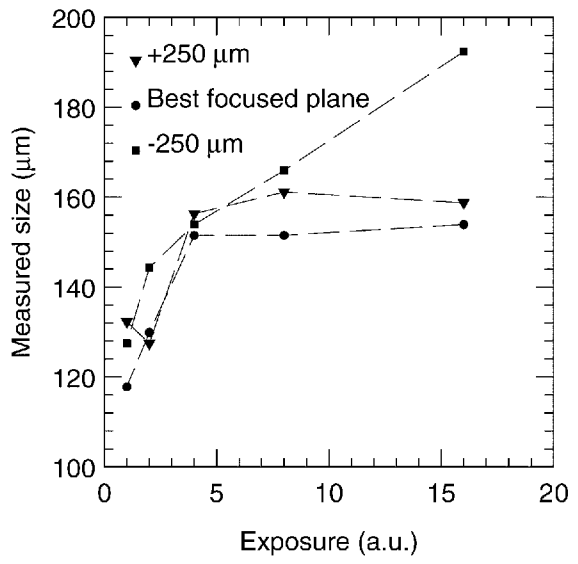

Fig. 7. Dependence of measured particle sizes on energy and defocusing in the PIV recording.

of the best focusing, along the optical axis. Several different exposure times were used for each plane. Particle images were overexposed on the highest exposures but underexposed on the lowest exposures. They look like the ones presented in Figs. 3 (e)-(h). Figure 7 shows the results obtained from measuring the size of the same specific particle in all the recordings.

Finally, the performance of the phase separation procedure has been studied using a test object that simulates a two-phase PIV recording (Fig. 8(a)). It is a computer printout of two size black dots on white paper. These dots are in groups of four of them equally spaced. There are about 10 times more small dots (continuous phase) than big dots (disperse phase). The test recording obtained, after photographing the object in the same conditions as with the previous computer printout objects, have an average of one group of big particle images per mm^2. The spacing of the dots is ~200 μm for both phases but in very different directions (50° and 30° for the disperse and continuous phases, respectively). Particle image sizes are 85 μm and less than 40 μm for each phase. Figures 8(b),(c) show the velocity vectors obtained from the continuous phase and from the disperse phase. As explained before, the phase separation is based on measured size. The very different velocity direction of both

phases is used to estimate the correlation between size and correct velocity. We have found that less than 10% of the data are incorrectly measured. Figure 8(b) clearly shows that simultaneous measurements of both phases are possible, since it has vectors in many points where the disperse phase has also been measured. Let us note that the missing vectors are due to small numbers of continuous phase tracer images. This is caused either by a locally low tracer concentration or by a reduced local tracer image concentration due to blocking by the disperse phase images. Figure 8(c) shows that, while the disperse phase is correctly identified, the accuracy of its positioning and the identification of individual particles still needs some improvement.

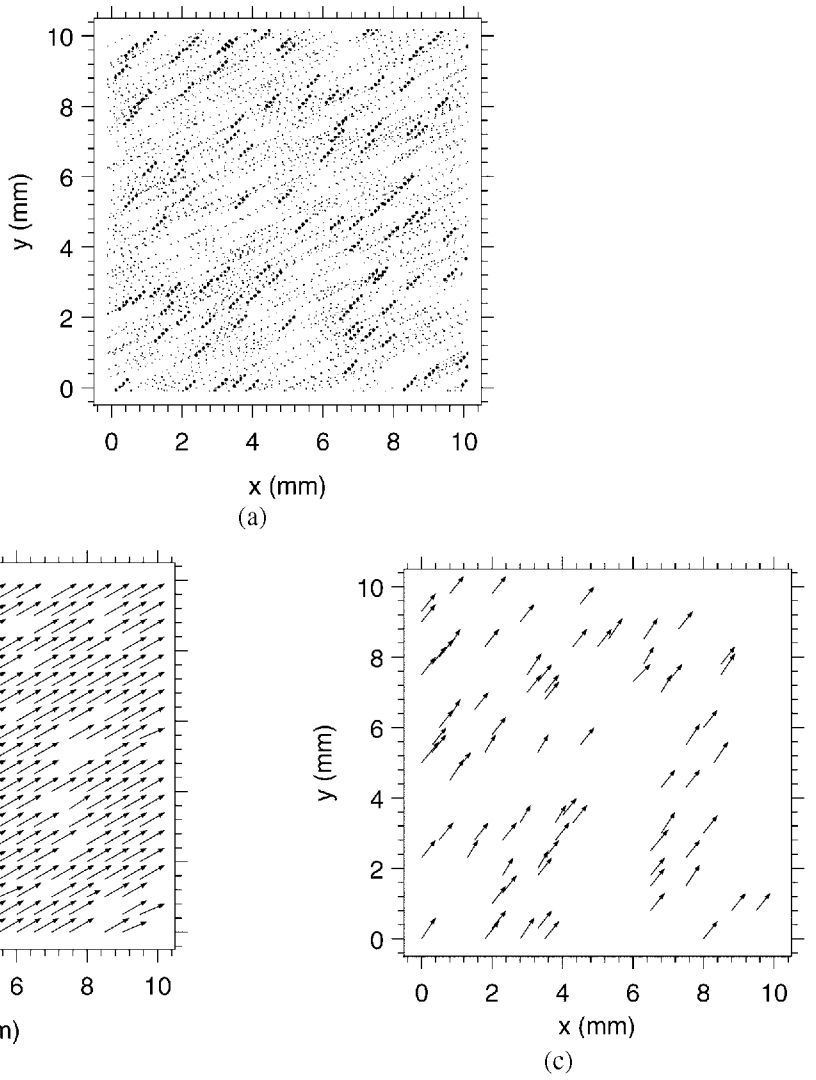

Fig. 8. Phase separation testing. (a) Computer generated test object with different velocity field for each phase; (b) continuous phase velocity field; (c) disperse phase velocity field.

4. Measurements in Air-solid Flow

In order to test the performance of the multiphase flow diagnostics, some experiments were carried out in a two-phase flow implemented at the University of Edinburgh. It consists on a particle-laden expanding airflow, formed by a fan, and fed into a vertical channel. The channel was made of glass and had a squared cross section of 55×55 mm^2. The airflow was travelling vertically up, leaded by the channel, with a velocity of about 6 m/s. The airflow was far from fully developed due to the short distance (about 1 m) between the expansion and the test section. The particles in the flow were solid glass spheres with diameters between 44 to 115 μm (mean value: 75 μm). The airflow was seeded with 1-2 μm corn oil droplets.

The air-particle flow field was illuminated by a pulsing light sheet from two double-Q-switched Nd:Yag lasers. A lens system converted the train of 4 pulsing beams into a train of collimated pulsing light sheets whose duration was 8 ns. The time interval between pulses was selected to be 50 μs. PIV recordings of the flow field were taken with a 4×5" format camera fitted with a Nikkor AM 120 mm lens set up for $M = 0.8$.

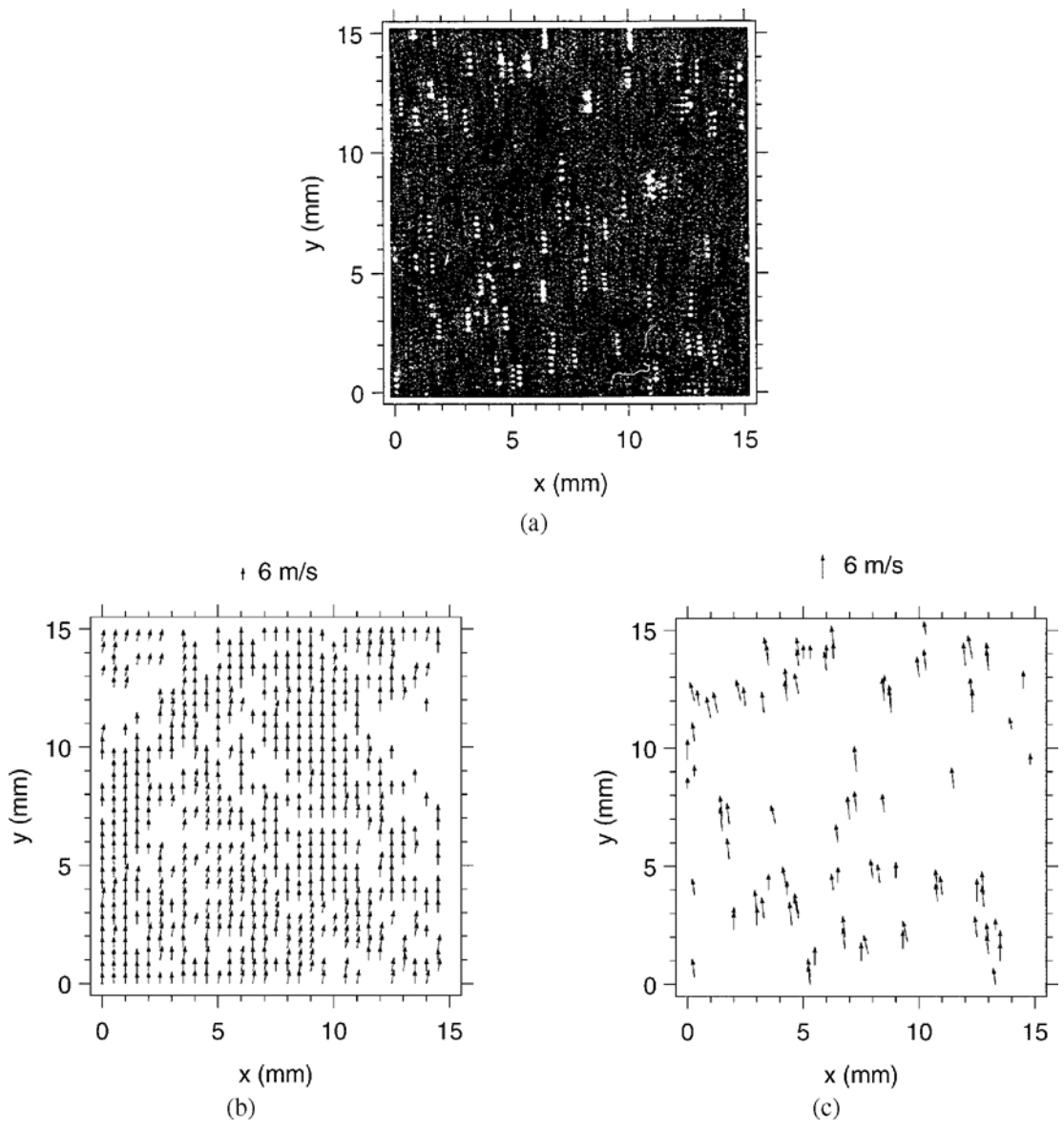

Fig. 9. Air-particle flow with a mean velocity of 6 m/s. (a) Raw PIV image; (b) velocity map of the air phase; (c) velocity map of the particle phase.

Figure 9 shows a 15×15 mm² area of a PIV image and corresponding velocity maps. Figure 9(a) clearly shows that the particle-phase images are more clearly seen than the air-phase images due to its bigger size. Particle images look circular and are probably overexposed because no care was taken to decrease the particle scattered light. Figure 9(b) shows the velocity map of the air-phase. Figure 9(c) shows the velocity map of the particle-phase. As a rough estimate, more than 90% of particle traces have been successfully measured as particles in this particular test. Sizes measured for those particles range from 75 to 200 μm with a mean value of 125 μm. These values are 1.7 times the nominal values, which confirms the overexposure of the particle images. It is encouraging that all the particle images are enlarged by the same factor. We believe that better size measurements are possible by a better control of the exposure of the particles.

5. Conclusions

A method of analyzing PIV recordings for multiphase flow diagnostics has been presented. Software has been developed to separate the measurements of the different phases. These measurements include velocity of all the phases and sizes (and may be concentration) of the disperse phases. The performance of the size diagnostics and the phase separation has been analyzed by using different test objects. Some parameters affecting the accuracy of the size measurements have been discussed. The multiphase flow diagnostics has been demonstrated in an air-particle flow where both phases have been discriminated and independently analyzed. The velocity field has been measured on the air-phase while velocity and particle sizes have been measured on the disperse phase. This research has shown the potential of the analysis method.

Acknowledgments

This work was partially funded by CICYT under grant AMB96-0427 and by the University of Zaragoza under the "Research Support Programme". We would like to thank Prof. Quintanilla for his many helpful discussions and Prof. Greated and Dr. Jakobsen for their involvement in the air-solid flow experiments.

References

Adrian, R. J., Particle-imaging Techniques for Experimental Fluid Mechanics, Ann. Rev. Fluid Mech., 23 (1991), 261-304.

Albert, R. and Farrell, P. V., Droplet Sizing using the Shifrin Inversion, J. Fluid Eng., 116 (1994), 357-362.

Arroyo, M. P., Yonte, T., Quintanilla, M. and Savirón, J. M., Velocity Measurements in Convective Flows by Particle Image Velocimetry using a Low Power Laser, Opt. Eng., 27 (1998a), 641-649.

Arroyo, M. P., Yonte, T., Quintanilla, M. and Savirón, J. M., Particle Image Velocimetry in Rayleigh-Benard Convection: Photographs with a High Number of Exposures, Opt. and Lasers in Eng., 9 (1988b), 295-316.

Chen, R. C. and Fan L. S., Particle Image Velocimetry for Characterising the Flow Structure in Three-dimensional Gas-liquid-solid Fluidized Beds, Chem. Eng. Sci., 47 (1992), 3612-3622.

Coil, M. A. and Farrell, P. V., Droplet Size and Velocity Measurements in a Spray, Proceedings of the Sixth International Conference on Liquid Atomization and Spray Systems 1994 (Rouen), 414-420, Begell.

Hassan, Y. A. and Canaan, R. E., Full-field Bubbly Flow Velocity Measurements using a Multiframe Particle Tracking Technique, Exp. Fluids, 12 (1991), 49-60.

Hassan, Y. A., Blanchat, T. K., Seeley, Jr., C. H. and Canaan, R. E., Simultaneous Velocity Measurements of Both Components of a Two-phase Flow using Particle Image Velocimetry, Int. J. Multiph. Flow, 18 (1992), 371-395.

Jakobsen, M. L., Easson, W. J., Greated, C. A. and Glass, D. H., Particle Image Velocimetry: Simultaneous Two-phase Flow Measurements, Meas. Sci. Technol., 7 (1996), 1270-1280.

Liu, Z. C. and Adrian, R. J., Simultaneous Imaging of the Velocity Fields of Two Phases, in Particulate Two-phase Flows, (1992), 33-58, ed. M. Roco, Butterworth, New York.

Palero, V., Jakobsen, M. L., Arroyo, M. P. and Quintanilla, M., Stereoscopic Particle Image Velocimetry for Size and Velocity Measurements in Multi-phase Flows, Proceedings of the Sixth International Conference on Industrial Metrology 1995 (Zaragoza), 462-470, Editorial Kronos.

Quiroga, J. A., González-Cano, A. and Bernabeu, E., Fast Method to Measure the Irradiance Response of Image Processing Systems, Meas. Sci. Technol., 6 (1995), 181-187.

Authors' Profiles

Virginia Palero: She was born in Spain in 1968. She received the master's degree in physics from the University of Zaragoza in 1991. She will get the doctorate degree later this year. Her graduate work involves the development and application of particle image velocimetry and holographic interferometry for the study of three-dimensional multiphase flows. She is presently a teaching assistant at the University of Zaragoza. Her main research interest lies on the field of optical measurements in fluids.

Pilar Arroyo: She received her master and doctorate degrees in physics from the University of Zaragoza in 1981 and 1987, respectively. Her graduate work involved the study of Rayleigh-Bénard convective flows by particle image velocimetry. She was a teaching assistant until 1992, when she became a professor of Applied Physics at the University of Zaragoza. She worked on stereoscopic particle image velocimetry in acoustic flows at the University of Edinburgh in 1990 and on tunable diode laser absorption spectroscopy for the detection of water vapor at the University of Stanford in 1991 and 1992. Her main research interests are on the development and application of optical techniques to fluid mechanics, with particular interest in velocimetry techniques such as particle image velocimetry and holographic interferometry.